Flexible Sustained Ionogels with Polymer Ionic Liquids for Enhanced Ion-Conduction and Energy Storage

*Paraskevi Flouda, Daria Bukharina, Kellina J. Pierce, Alexandr V. Stryutsky, Valery V. Shevchenko, and Vladimir V. Tsukruk**

Paraskevi Flouda, Daria Bukharina, Kellina J. Pierce, and Prof. Vladimir V. Tsukruk*

School of Materials Science and Engineering, Georgia Institute of Technology, Atlanta, Georgia 30332, USA.

*E-mail: vladimir@mse.gatech.edu

A. V. Stryutsky, Prof. V. V. Shevchenko

Institute of Macromolecular Chemistry of the National Academy of Sciences of Ukraine, Kharkivske Shosse 48, Kyiv 02160, Ukraine.

Abstract

Flexible and mechanically robust gel-like electrolytes offer enhanced energy storage capabilities, versatility, and safety in batteries and supercapacitors. However, the trade-off between ion-conduction and mechanical robustness remains a challenge for gel-like electrolytes. Here, we suggest that the introduction of hyperbranched polymer ionic liquids (PILs) in structured sustained ionogels will lead to both enhanced ion-conduction and mechanical performance due to the PILs' ionically conductive bearing groups and the complementary interfacial interactions with ionic liquids. More specifically, we investigate the effect of hyperbranched PILs with carboxylate terminal groups and imidazolium counterions with various ionic group densities on the properties of ionogels composed of co-assembled cellulose nanofibers (CNFs) and cellulose nanocrystals (CNCs) as sustainable open pore frame for ionic liquid immersion. The addition of PILs leads to the formation of highly interconnected open porous, lightweight, and shape-persistent materials by harnessing hydrogen bonding between PILs and CNFs/CNCs "frame". Notably, these materials possess a two-fold improvement in ionic conductivity combined with many-fold increase in Young's modulus, tensile strength, and toughness making them comparable to reinforced elastomeric materials. Furthermore, the corresponding thin-film gel-based supercapacitors possess enhanced electrochemical cycling stability upon repeated bending with a 85% capacitance retention after 10000 cycles promising new insight in the development of simultaneously conductive and flexible, robust gel electrolytes with sustained performance.

Keywords: *Sustainable gel electrolytes, polymer ionic liquids; cellulose nanofibers; cellulose nanocrystals, flexible supercapacitors*

1. Introduction

The growing demand for portable electronics and electric vehicles has led to the need for more efficient and safer energy storage devices.[1] An important performance-determining component in energy storage devices is the electrolyte material that plays a critical role in the ion transport dynamic between electrodes and their trapping in their vicinity.[2] Among the different electrolytes, ionic liquids have received great attention due to their exceptional performance and prospective for safe and high capacity energy storage.[3] As known, ionic liquids are viscous molten salts composed of cations and anions with a melting temperature below 100°C.[3] They possess a high operational potential window (3 – 3.5 V), relatively high ionic conductivity (1 – 15 mS/cm), low-volatility, and high thermal and chemical stability.[3] Recent studies on ionic liquids focused on increasing their operational potential window, as well as on integrating them in different electrochemical energy storage devices including supercapacitors, lithium-ion, dual-ion, and sodium-ion batteries.[3, 4, 5] However, concerns with leakage of ionic liquids, corrosion of the packaging materials, toxicity, their viscous fluidic nature, and inability to preserve a sustainable shape under external and internal stresses caused by cyclical and occasional thermal, deformational, and electrical variances hinder their extended utilization in future energy storage applications.[3]

To overcome these critical challenges, integrating ionic liquid molecules into polymer chains to form polymerized ionic liquids (PILs) and/or incorporating ionic liquids inside mechanically robust porous solid matrices have been suggested.[3] As known, PILs carry ionic liquid species at their repeated units synthesized by the direct polymerization of ionic liquids or the chemical modification of existing polymers.[6] PILs retain most properties of their ionic liquid precursors, while offering mechanical stability and dimensional control.[6] Their properties depend on various parameters, such as the branched macromolecular architecture, the length of the alkyl chains, the nature of the ionic liquid species, and the ionic group density.[7, 8] However, PILs demonstrate lower ionic conductivity (< 1 mS/cm) due to the partial immobilization of the ionically conductive groups and sluggish polymer chain mobilities.[7]

As an alternative to PILs, recent studies suggested incorporating ionic liquids inside supporting organic and inorganic materials.[9, 10] Using this method, the resulting composites combine the high ionic conductivity of the ionic liquids with the mechanical robustness of the host materials.[9, 10]

Host materials include epoxy, cellulose, and organosilane networks.[9, 10] For example, epoxy-based electrolytes containing 50 wt% 1-butyl-3-methylimidazoliumbis (trifluoromethylsulfonyl)imide ([BMIM][TFSI]) as the ionic liquid, bis(trifluoromethane)sulfonimide lithium salt (LiTFSI), and Al_2O_3 nanowires as reinforcements exhibited an ionic conductivity of 8.6 mS/cm, a Young's modulus of 0.6 GPa, and a tensile strength of 6.5 MPa.[11] However, efforts to further improve the mechanical performance of composite ionogels to make them stress-sustaining materials for energy storage led to dramatically deteriorated ionic conductivities, as these properties come at a trade-off.[11]

Cellulose nanofiber networks have shown great promise as host framework structures for shape-persistent gel electrolytes. Gel-like structures composed of cellulose nanofibers (CNFs) and cellulose nanocrystals (CNCs) demonstrate enhanced mechanical properties and high porosity.[12, 13] More specifically, CNFs combined with 95 wt% 1-ethyl-3-methylimidazolium bis-(trifluoromethylsulfonyl)imide ([EMIM][TFSI]) exhibited high ionic conductivity values (5.7 mS/cm) with good thermal stability (until 300 ºC) and a storage modulus of 5 MPa.[12] Recently, the incorporation of 95 wt% ionic liquids in a matrix of CNCs and PILs has been demonstrated.[12] The resulting composite ionogels exhibited high ionic conductivity values (7.8 mS/cm) with an increased compressive modulus of 5.6 MPa and a compressive strength of 0.8 MPa, common for rubbery materials.[12] However, a better understanding of how the incorporation of PILs with different ionic group density can affect the energy storage performance along with higher mechanical robustness is crucial for enhancing ionic, electrochemical, and mechanical properties relevant to demanding energy storage materials.

Here, we investigate for the first time the effect of hyperbranched PILs with various ionic group densities on the ionic conductivity, mechanical performance, and final energy storage performance in a solid-state supercapacitor of sustained CNF/CNC ionogels (**Figure 1a** and **Figure S1**). Hyperbranched PILs with carboxylate terminal groups and imidazolium counterions with various ionic group densities were selected due to their chemical affinity to CNFs/CNCs and the commonly used [EMIM][TFSI] ionic liquids. CNFs were used to create continuous porous networks with abundant surface groups available for hydrogen bonding while CNCs acted as mechanical reinforcements.[14] The co-assembly of CNFs and CNCs led to the formation of mechanically robust open porous continuous networks, able to host large amounts of ionic liquids (up to 90 wt%). Multi-fold and concurrently improved ion-conductivity, Young's modulus, tensile

strength, and toughness make these electrolytes comparable to tough reinforced elastomeric materials without damping ion conductivity and electrochemical performance. The synergetic effects of the assembly of the mechanically robust CNF/CNC networks and the ionically conductive hyperbranched PILs were enhanced by increasing the PIL ionic group density and harnessing the strong interfacial interactions between the PILs and the CNF/CNC networks. Finally, exploring these composite ionogels in solid state supercapacitors showed a high cycling stability with an up to 85% capacitance retention upon 10000 cyclic bending deformations and demonstrated their potential for energy storage applications.

2. Materials

Synthesis of PILs: PILs with hyperbranched cores and 16 (PIL-16), 32 (PIL-32), and 64 (PIL-64) carboxylated terminal groups and imidazolium counterions were synthesized in three steps starting from the acylation of aliphatic hyperbranched oligoester polyols containing terminal primary hydroxyl groups, as previously reported from our group.[15] Detailed chemical synthesis steps are included in our prior publications and in the Supporting Information, **Figure S1**).[15] Ionic liquid, 1-ethyl-3-methylimidazolium bis-(trifluoromethylsulfonyl)imide ([EMIM][TFSI], 99%) was purchased from Iolitec-Ionic Liquid Technologies (**Figure 1a**).

Preparation of cellulose nanofibers: Wood pulp was purchased from Georgia Pacific LLC. CNFs were prepared from wood pulp through TEMPO-oxidation followed by intensive tip sonication, as previously reported.[14] More specifically, wood pulp torn pieces (1 g) were washed with deionized (DI) Milli-Q water, followed by air-drying. The wood pulp pieces were suspended in water (100 ml) containing TEMPO (0.016 g) and NaBr (0.1 g). The mixture was stirred at room temperature and its pH was continuously monitored using a pH probe. To trigger the TEMPO-oxidation, a small amount (6 ml) of NaClO solution was added to the mixture. The pH was adjusted to 10 using 1M NaOH and 1M HCl aqueous solutions. Once NaClO was fully consumed and the pH was stabilized at 10, the mixture was washed thoroughly with DI water and subjected to tip sonication (Qsonica Q700 with 1.2 cm diameter probe, 40% amplitude, 5 sec on/off) for 30 minutes. Finally, the mixture was centrifuged for 30 minutes at 10,000 rpm to yield a CNF dispersion of a concentration of 0.44 wt%.

Preparation of cellulose nanocrystals: CNCs were prepared through sulfuric acid hydrolysis.[12],[16] More specifically, wood pulp pieces (34 g) were hydrolyzed using 64 wt % H_2SO_4 (300 ml)

at 45 ºC for 1h under stirring. The solution was diluted with DI water (to 2800 mL) and left undisturbed overnight to separate the hydrolyzed wood pulp from water. The wood pulp suspension was centrifuged twice at 6000 rpm for 5 min to remove the remaining acid. The supernatant was discarded, while the sediment was collected, redispersed in 1200 mL DI water, and dialyzed against water using cellulose dialysis tubing (12000 – 14000 MWCO, Thermal Scientific) for two weeks. Two more rounds of centrifugation at 1100 rpm for 20 min were performed. Finally, the supernatant was tip-sonicated at 40% amplitude, 5 s on/5 s off, for 4 min and 30 sec using a large tip sonicator (Qsonica Q700 with 1.2 cm diameter probe).

Preparation of composite ionogels: CNF and CNC dispersions were concentrated through water evaporation to 1.5 wt% and 3 wt%, respectively. CNC dispersions were added to CNFs at desired concentrations (0 wt%, 5 wt%, 10 wt%, and 15 wt%) under intensive stirring for 2h, followed by 1h of bath sonication. The mixtures were drop-casted in glass petri dishes of 3 cm in diameter. Water/ethanol exchange was performed to remove the water by carefully adding ethanol (2 ml) on the top of the solutions/hydrogels and replacing it every 3h for 5 days, until no refractive index gradients were observed. Small amounts (0.6 g) of ionic liquid, [EMIM][TFSI], were mixed with 2 ml ethanol and added in the samples. The gels were left undisturbed overnight, followed by slow ethanol evaporation for a week. Finally, the ionogels were dried overnight at 70 ºC under vacuum. Freely-standing ionogel films with a thickness of 150 – 300 μm and diameters of ~2.5 cm were obtained. To fabricate composite ionogels containing PILs, small amounts (50 μl) of 12 wt% PILs in water were added in the CNF/5 wt% CNC mixtures, followed by the same procedure.

Sulfuric acid (H_2SO_4, ACS reagent, 95 – 98%), sodium bromide (NaBr, ACS reagent, ≥ 99%), hydrochloric acid (HCl, ACS reagent, 37%), sodium hydroxide (NaOH, reagent grade, ≥ 98%, pellets (anhydrous)), sodium hypochlorite solution (NaClO, reagent grade, 10 – 15%), and (2,2,6,6-tetramethylpiperidin-1-yl)oxyl (TEMPO, 98%) were purchased from Sigma-Aldrich.

Chemical and morphological characterization: Attenuated total reflectance Fourier transform infrared (ATR-FTIR) spectra were collected using a Bruker Vertex 70 FTIR spectrophotometer (1200-4000 cm^{-1}) with the resolution of 4 cm^{-1} and the number of scans of 200. Proton nuclear magnetic resonance (^1H NMR) spectra were recorded with Varian VXR-400 MHz spectrometer using DMSO-d_6 as a solvent. Zeta-potential was measured with Zetasizer Nano Z (Malvern Instruments) in polystyrene cuvettes and measurements were repeated three times.

X-ray photoelectron spectroscopy (XPS) measurements were conducted using a Thermo K-Alpha XPS (Thermo Scientific) with Al Kα radiation (hm = 1486 eV). For the survey scans, two scans were collected with a step of 1.0 eV and dwell time of 50 ms. For high-resolution scans, 10 scans were collected with a step of 0.1 eV and dwell time of 50 ms. Finally, a Shirley background correction was performed, followed by a Gaussian-Lorentzian peak shape fitting. Deconvolution of the high-resolution peaks was performed by constraining the FWHM of the deconvoluted peaks. All spectra were calibrated based on the C1s peak for sp^2-hybridized carbon atoms at 284.5 eV, as typically done for cellulose-based materials.[17, 18, 19]

UV-Vis spectroscopy measurements from 300 - 800 nm were conducted with a Shimadzu UV-3600 Plus Spectrophotometer.

Thermal gravimetric analysis (TGA) was conducted using Q600 STD (TA Instruments). All samples were dried overnight at 80 ºC under vacuum prior testing and 8 – 10 mg of each sample were placed in an aluminum pan. The samples were heated from room temperature to 600 ºC at a heating rate of 10 ºC/min under nitrogen gas.

AFM was conducted using an Bruker Dimension Icon microscope operated in standard tapping mode in air.[20] AFM probes (HQ:XSC11/AI BS) with a tip radius of 8 nm and a spring constant of 1.1 – 5.6 N/m were used. The scan rate was 1.0 Hz and the resolution of the AFM images was set to 512 x 512 pixels. AFM was conducted on drop-casted samples (100 µl of the hydrogel mixtures or 100 µl of diluted to 0.01 wt% hydrogel mixtures) on silicon substrates (UniversityWafer, piranha treated)

SEM was performed on aerogels (without ionic liquids) and the as-prepared ionogels. The aerogels were prepared by drying the organogels (in ethanol) using CO_2 critical point drying (EMS 850 critical point dryer). SEM images were taken on a Hitachi SU-8230 microscope operated at 3kV. Samples were sputter-coated with gold for 60 sec at 30 mA.

Mechanical characterization: Tensile tests were conducted using a Shimadzu EZ-SX tester with a displacement rate of 1 mm/min. The samples were cut into 5 x 10 mm strips using a razor blade. All experiments were conducted at room conditions (temperature: ~ 23 ºC and RH: 35 - 48%) and 5-7 specimens were tested per composition.

Ionic conductivity measurements: Electrochemical impedance spectroscopy (EIS) was performed in two-electrode coin cells to evaluate the ionic conductivity of the ionogels. More specifically, the ionogels were punched into 19 mm in diameter circles and placed between two stainless-steel blocking electrodes. The potential was oscillated at 0 V vs. the open circuit potential (OCP) with an AC amplitude of 10 mV and a frequency range of 1 mHz – 1 MHz using a Bio-logic SAS potentiostat. The ionic conductivity (σ) was calculated from the equation: $\sigma = t/R \cdot S$, where t is the ionogel film thickness, R is the bulk resistance obtained from EIS, and S is the ionogel surface area in contact with the electrodes.[21]

Electrochemical properties: Electrochemical characterization was conducted in two-electrode symmetric pouch cells using two reduced graphene oxide films as the electrodes and the ionogels as the electrolytes. GO dispersions in water were prepared from graphite powder (325 mesh, Alfa Aesar) using a modified Hummers method.[22, 23] GO dispersions (40 ml of 1 mg/ml) were vacuum filtered using a Nylon membrane (diameter: 47 mm and pores: 200 nm). The films were washed with DI water, peeled-off the filter paper, air-dried overnight, and oven dried under vacuum at 80 ^{o}C for 3 days. Thermal reduction was performed at 200 ^{o}C under vacuum to yield rGO films.

The rGO electrodes were cut into 1.8 cm x 1.8 cm squares (mass: ~ 9 mg and thickness: ~ 30 μm) and were attached to a double-sided carbon conductive tape (3M XYZ-Axis) that acted as a current collector. The ionogels (2.0 cm x 2.0 cm) were placed in-between two rGO electrodes, and a polyimide tape (Bertech) was used to wrap the supercapacitor and provide external electrical insulation. The total mass and thickness of the devices were ~ 500 mg and ~ 0.5 mm, respectively.

Cyclic voltammetry was performed using the pouch cells at varying scan rates from 1 mV/s to 100 mV/s within a potential window of 0 – 3 V. All cells were pressed to ensure good contact between the different layers, left undisturbed overnight, and preconditioned with a potentiostatic step at 3V vs. OCP for 5 mins and 10 cyclic voltammetry cycles at 20 mV/s. Three cells were tested per ionogel composition. The specific capacitance of one electrode was calculated from cyclic voltammetry using the equation: $C = 2 \cdot \int_{V_{min}}^{V_{max}} \frac{I}{v \cdot \Delta V \cdot m} dV$, where I is the current, V is the voltage, ΔV is the potential window, m is the mass of two electrodes, and ν is the scan rate.[24] Galvanostatic charge-discharge experiments were conducted at 0.2 A/g and the specific capacitance of one electrode was calculated using the equation: $C = 4 \cdot \frac{I \cdot \Delta t}{m \cdot \Delta V}$, where Δt is the

discharge time, as previously reported.[24] The specific energy of the device was calculated from the equation: $E = \frac{1}{8} \cdot C \cdot \Delta V^2$.[24]

3. Results and discussion

Synthesis and preparation of all materials components is described in **Methods**. AFM images of CNFs revealed nanofibrillar structures with diameters of 3 – 4 nm and lengths up to 0.5 µm, while CNCs exhibited needle-like structures with diameters of ~ 6.1 nm and length of ~ 165 nm (**Figure 1b**), as reported earlier.[14] AFM images of drop-casted pure PIL-16, PIL-32, and PIL-64 (**Figure 1b** and **Figure S2**) showed nanodroplets of a few tenths of nanometer in diameter. FT-IR spectra of the TEMPO-oxidized nanocelluloses exhibit a prominent peak at 1618 cm^{-1} due to vibrations from the carbonyl groups, and the CNCs exhibit all characteristic features for processed nanocelluloses (**Figure S3a**).[15]

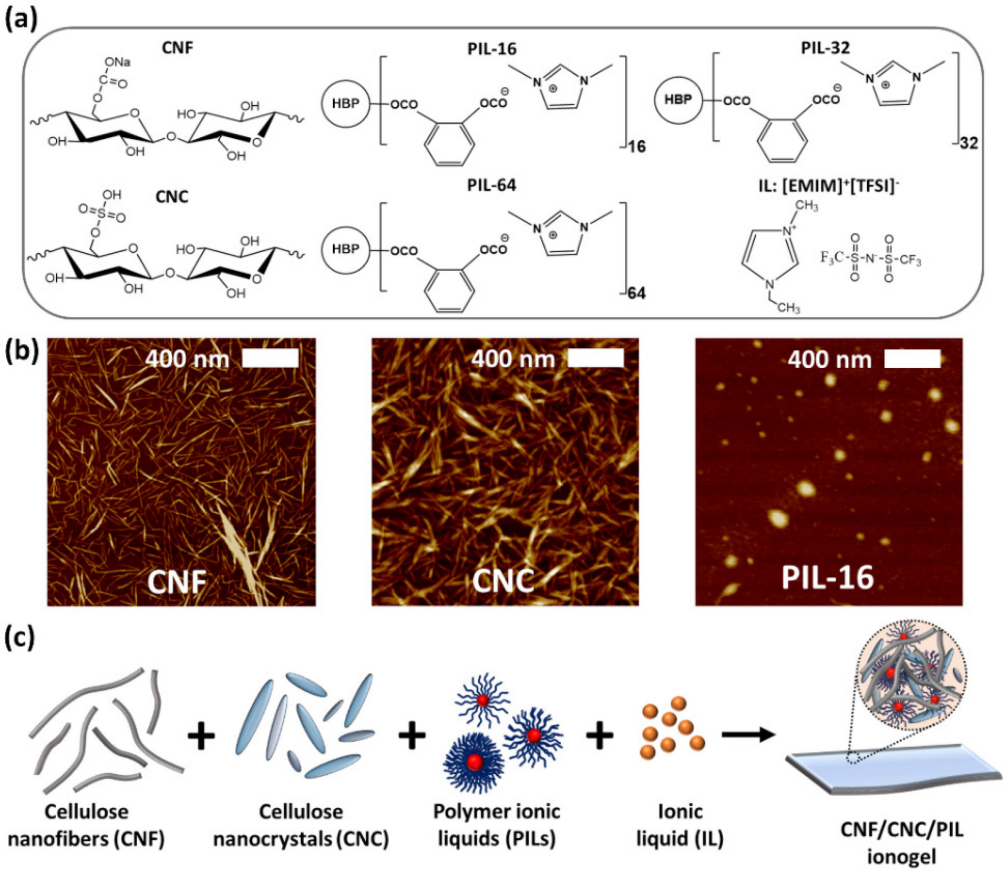

Figure 1. (a) Chemical structures of material components and (b) corresponding AFM topography images. The Z-scale is 10 nm, 25 nm, and 6 nm for CNF, CNC, and PIL-16, respectively. (c) The step-by-step assembly pathway for fabrication of robust ionogels from CNF + CNC with added PILs and ionic liquids (from left to right).

For assembly of reinforced ionogels we explored PILs containing polyol hyperbranched cores with 16 (PIL-16), 32 (PIL-32), and 64 (PIL-64) carboxylated terminal groups and imidazolium counterions (**Figure 1a** and **Figure S1**).[12, 15, 25, 26] The PILs investigated in this study belong to a special class of branched polyelectrolytes. [15, 27] Contrary to the traditional linear polyelectrolytes where a considerable portion of the constitutional units contain ionic or ionizable groups, these PILs are composed of multiple branches containing terminal ionic groups and counter ion liquid species (**Figure 1a**). [15, 27]

The chemical composition of the PILs was confirmed by both ^{1}H NMR and FT-IR spectra (see Supporting Information, **Figure S4, S5,** and **Figure S3b**). The ^{1}H NMR spectra contain characteristic signals of aliphatic hyperbranched oligoester cores and aromatic components. Specifically, signals of methyl groups of hyperbranched cores (0.84 – 1.25 ppm), aromatic rings of benzene and imidazolium (7.21 – 8.57, 9.15 ppm), and methyl groups of imidazolium cations (3.83 – 3.84 ppm) were observed. Also, the proposed structure of the PILs was evidenced by the ratios of the integrals of the corresponding proton signals in the NMR spectra. The FT-IR spectra of all PILs confirmed their chemical composition by exhibiting the characteristic peaks/absorption bands, such as stretching modes of C=O bonds at 1716 – 1720 cm^{-1}, symmetric and asymmetric vibrations of bonds of $(COO)^-$ carboxylate anions at 1379 – 1396 cm^{-1} and 1568 – 1605 cm^{-1}, and oscillations of the imidazolium bonds (C–H bonds in 2nd position of imidazolium cation) and hydrogen bonding at 3100 – 3600 cm^{-1} (**Figure S3b**).[15]

Initially, CNF/CNC ionogels without PILs were fabricated to determine the optimum CNC composition. More specifically, concentrated CNF aqueous dispersions were mixed with CNCs, followed by water/ethanol exchange, and the addition of ionic liquids (ILs, [EMIM][TFSI]). Ionogels containing 0.5 wt% CNC were selected for further studies due to their improved mechanical performance (tensile strength, Young's modulus, toughness, and ultimate strain), as shown in **Table S1** and **Figure S6** and discussed in section 3.3. Below, 'CNF/CNC' implies a content of 0.5 wt% CNC. For the PIL-containing ionogels, aqueous mixtures of the different PILs were added in the CNF/CNC suspension (**Figure 1c**). Aqueous CNF/CNC/PIL mixtures formed hydrogels faster than the CNF/CNC mixtures that did not contain PILs (**Figure S7**). More specifically, CNF/CNC/PIL-32 and CNF/CNC/PIL-64 formed a hydrogel within 15 min. Mixtures containing PIL-16 formed gels within an hour, while the CNF and CNF/CNC mixtures (without PILs) required several hours for formation.

3.1 Properties and morphology of composite ionogels

During assembly, uniform gelation without phase separation occurred despite the negatively charged groups that CNFs, CNCs, and PILs possess (carboxylate and sulfate groups). This indicates that CNF/CNC and PIL assembly resulted from extensive hydrogen bonding between the different components, as also confirmed by XPS data discussed in section 3.2. Indeed, the negative surface charges of CNF, CNC, and PILs, were confirmed by zeta-potential measurements (**Figure S8**). CNF aqueous mixtures demonstrated a zeta-potential of -39.5 ± 5.0 mV, and upon addition of CNCs the zeta potential changed to -43.5 ± 5.0 mV due to the more negative surface charge of cellulose nanocrystals (-51.7 ± 1.0 mV) similarly to those reported earlier.[28] The introduction of PILs in the CNF/CNC aqueous mixtures led to increased zeta-potential negative values due to partial adsorption of the PILs on the carboxy-rich CNF/CNC surfaces.[12] Additionally, with increasing the PIL ionic group density, the negative zeta-potential values further reduced to -34.1 ± 1.0 mV, indicating greater presence of PIL with lower negative potential (**Figure S8**). The faster gelation rates and the reduced negative zeta-potential values for the PIL-containing mixtures suggest the formation of strong interfacial interactions between the PILs and CNF/CNC arising mainly from hydrogen bonding among different material components rather than electrostatic interactions.

In the end, free-standing films with thicknesses of ~ 300 μm were obtained by releasing from Petri dish (**Table 1**, **Figures 1c, 2a**, and **Figure S9**). The films were semi-transparent with an optical transmittance in visible range up to 50% (**Figure 2b**).

Table 1. Composition of CNF/CNC/PIL ionogels.

Ionogels	CNF [wt%]	CNC [wt%]	PIL [wt%]	IL [wt%]
CNF (IL)	10.0	-	-	90.0
CNF/CNC (IL)	9.5	0.5	-	90.0
CNF/CNC/PIL-16 (IL)	9.5	0.5	2.0	88.0
CNF/CNC/PIL-32 (IL)	9.5	0.5	2.0	88.0
CNF/CNC/PIL-64 (IL)	9.5	0.5	2.0	88.0

The films were mechanically robust, and shape persistent and not fluidic despite the high content of ionic liquids in the thin films (~ 90 wt%) (**Table 1**). Finally, the CNF/CNC/PIL-16 ionogels are flexible and can sustain folding, whereas the other composite ionogel films start cracking during folding (compare **Figure 2a** and **Figure S9**).

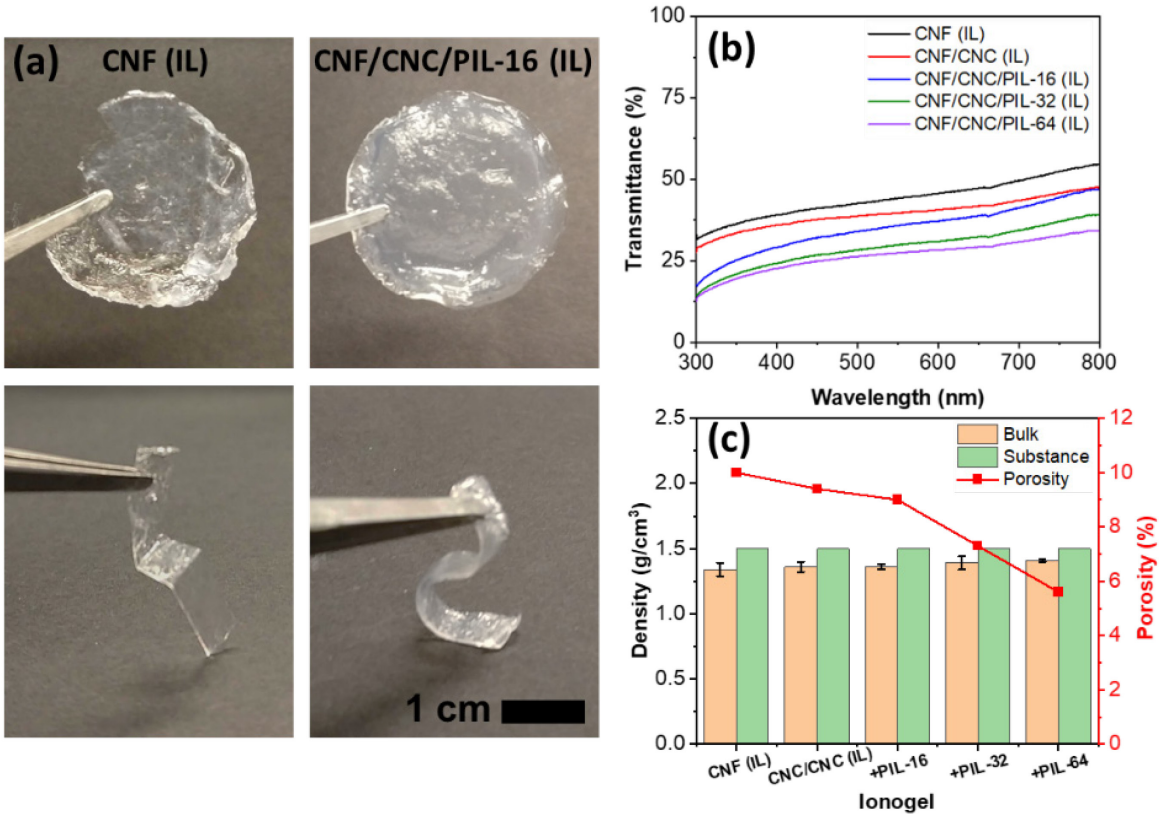

Figure 2. (a) Optical images for CNF (IL) and CNF/CNC/PIL-16 (IL). (b) Optical transmittance and (c) bulk and substance densities, and porosity for the composite ionogels.

The theoretical densities compared to experimental values to estimate their bulk porosity (**Figure 2c** and **Table S2**). More specifically, the bulk densities were calculated using the dimensions and mass of the ionogels, while the theoretical densities were calculated considering only solid and liquid phases.[29] An increase (from 1.34 g/cm^3 to 1.41 g/cm^3) in the bulk density values with the addition of CNCs and PILs was observed indicating the porosity decreasing from 10% for CNF ionogels to 5.6% for the composite ionogels (**Table S2**). The changes in bulk density and porosity values indicate the formation of denser ionogels due to strong interfacial interactions between CNF/CNC and PILs as was suggested by surface potential measurements as discussed

above. Additionally, the low porosity values indicate that most of the open free space inside the initial nanocellulose networks is mostly filled with added ionic liquid phase.

Large-scale morphology of composite ionogels was revealed by SEM imaging (**Figure 3a-c** and **Figure S10**). All CNF-based materials exhibited highly porous morphologies composed of open continuous CNF networks able to confine ionic liquids. CNC aerogels demonstrate porous interconnected structures as demonstrated earlier.[12] Aerogels containing both CNCs and PILs demonstrated more interconnected structures compared to pure CNF aerogels. SEM imaging of the ionogels was challenging and the nanoscale CNF/CNC features were not visible due to the high ionic liquid content (88 – 90 wt%) (**Figure 3a**). Therefore, SEM was performed on dried gels using CO_2 critical point drying (CPD) before the addition of ionic liquids.[30] Similarly, AFM imaging revealed continuous interconnected networks for various compositions with similar organization and fibrillar bundles forming open pores (**Figure 3d-f** and **Figure S11**).

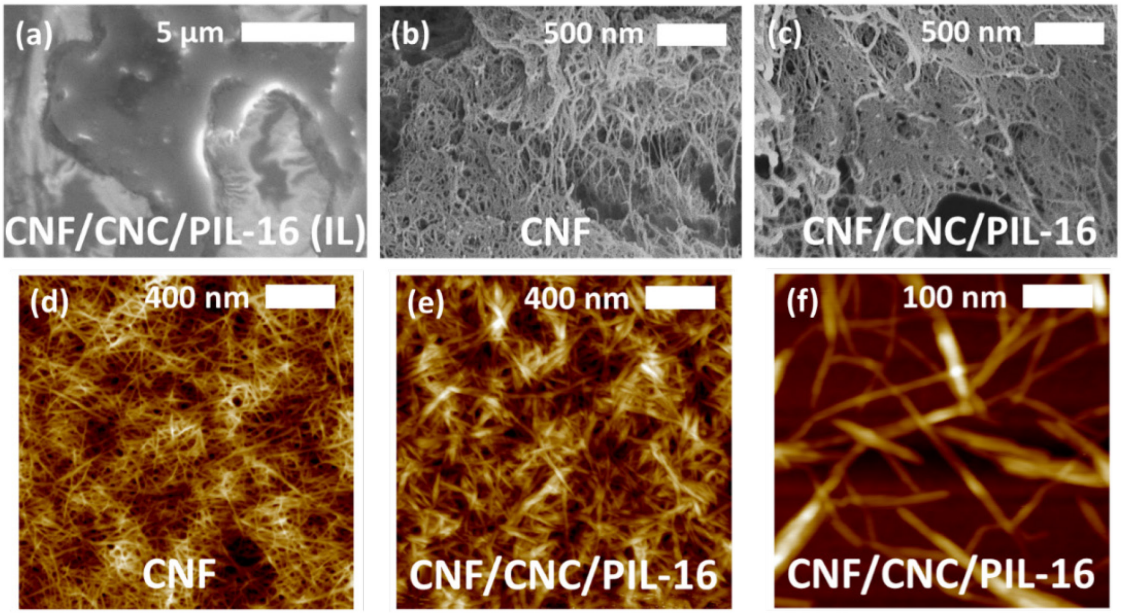

Figure 3. SEM images for CNF/CNC/PIL-16 (IL) ionogel, (b) CNF aerogel, and (c) CNF/CNC/PIL-16 aerogel. AFM images for (d) CNF, (e) CNF/CNC/PIL-16, and (f) zoomed-in AFM image for diluted (to 0.01 wt%) CNF/CNC/PIL-16 drop-casted samples on Si substrates. The Z-scale is 39 nm, 42 nm, and 17 nm for panels (d), (e), and (f), respectively.

3.2 Chemical composition, interfacial interactions, and thermal stability

The CNF-based ionogels exhibited FT-IR spectra similar to those of pure ionic liquid with peaks at 1200 – 1227 cm^{-1} due to symmetric and antisymmetric -CF_3 stretching vibrations and a -SO_2

antisymmetric stretching peak at 1354 cm^{-1}, verifying the addition of ionic liquid phase (**Figure S12**).[31] XPS study confirmed that initial CNF films (without ionic liquids) are composed of 67.1 at% carbon and 32.0 at% oxygen as expected from chemical composition (**Figure 4a** and **Table S3**).[32] Additionally, traces of sodium (0.9 at%) were found resulting from the TEMPO-oxidation process and the formation of sodium carboxylate (-COONa) groups (**Figure S13** and **Table S3**).

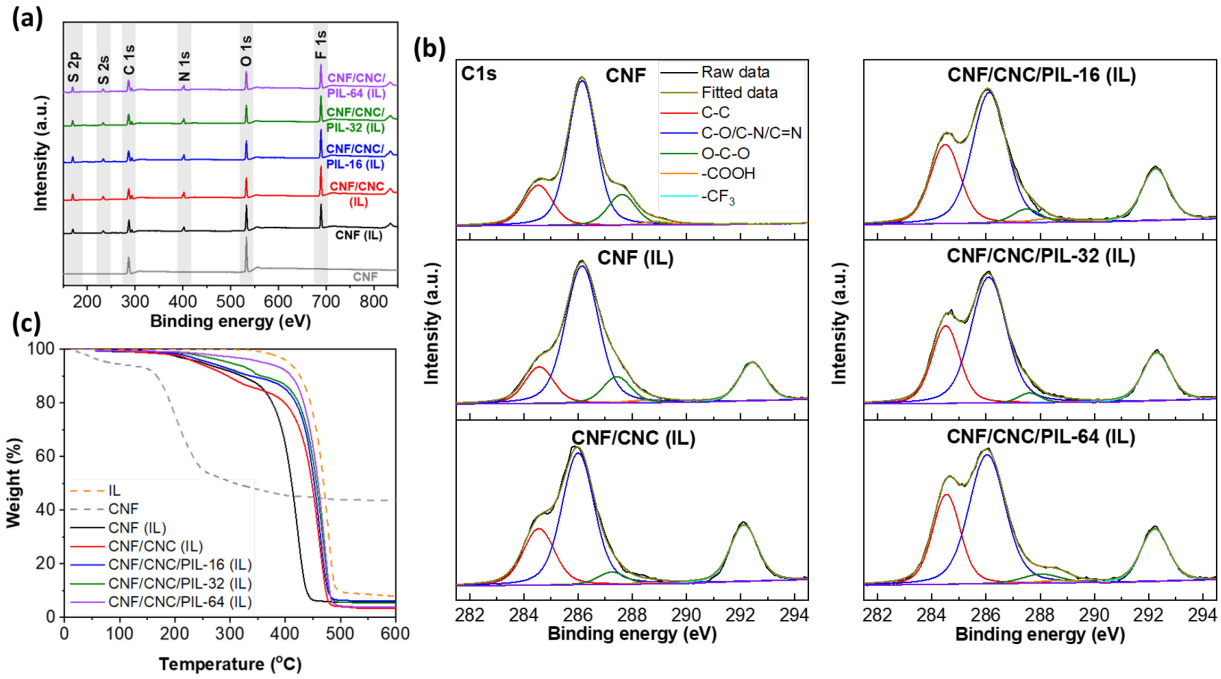

Figure 4. (a) XPS survey scans, (b) high-resolution C1s peaks, and (c) TGA for CNF, CNF (IL) CNF/CNC (IL), CNF/CNC/PIL-16 (IL), CNF/CNC/PIL-32 (IL), and CNF/CNC/PIL-64 (IL).

The incorporation of ionic liquids was verified by the appearance of additional peaks assigned to characteristic elements such as nitrogen, sulfur, and fluoride while the C/O ratio decreased to 1.7 (vs. 2.1 for pure CNF) (**Figure 4b**).[12, 33] Similar contents of sulfur (7.2 – 7.7 at%) and fluorine (22.8 – 23.1 at%) were found in all films indicating the incorporation of comparable amounts of ionic liquids. PIL-containing composite ionogels (CNF/CNC/PIL-16, CNF/CNC/PIL-32, and CNF/CNC/PIL-64) exhibited an increased C/O ratio (up to 2.3 vs.1.8 for CNF/CNC (IL)) due to the presence of terminal aliphatic chains (**Table S3**).

High-resolution C1s and N1s deconvoluted peaks for CNF films and the ionogels are shown in **Figure 4b**, **Table S4, Figure S14**, and **Table S5**. Pure CNF films (no ionic liquids) showed peaks associated to C-C, C-O, O-C-O, and -COOH/-COONa at 284.5 eV, 286.1 eV, 287.7 eV, and 288.7 eV, respectively.[12, 33] Addition of ionic liquids led to the appearance of a peak at ~292.4 eV

attributed to the -CF_3 groups of the ionic liquid [TFSI]. In all composite ionogels, the peaks attributed to the -CF_3 groups were shifted to lower binding energies compared to pure [EMIM][TFSI] (from 293.2 eV to ~ 292.4 eV) resulting from the confinement of the ionic liquids and the chemical interactions occurring between the ionic liquids and the CNF, CNC, and PIL functional groups.[12, 34] Similar peak shifts were observed in the high-resolution N1s peaks, as shown in **Figure S14** and **Table S5**. The N1s peaks were deconvoluted to two peaks at 399.4 eV and 402 eV attributed to the imide of the anion and the imidazolium ring of the cation.[34] The N1s peaks were shifted to lower binding energies (from 399.7 eV and 402.3 eV) as expected.[34]

As known, multiple weak chemical interactions including electrostatic interactions and hydrogen bonding can lead to shifts in the XPS deconvoluted peaks.[34] The negative zeta-potential values for CNFs, CNCs, PILs and their mixtures indicate that hydrogen bonding interactions are dominant within the gels before the addition of ionic liquids. More specifically, CNFs and CNCs interact with each other through hydrogen bonding interactions between their oxygen-containing groups.[14] Similar interactions occur between CNF/CNC and PILs with the CNF/CNC C-H and O-H groups interacting with the π^+-cloud in the PIL imidazolium ring.[12] Additionally, anionic CNC sulfonate and CNF carboxylate groups interact electrostatically with the imidazolium counterions of the PILs.[12] Addition of ionic liquids leads to the formation of ionic bridges between the ionic liquid [TFSI] anions and the PIL imidazolium counterions, as well as between the negatively charged groups in branches and the imidazolium counter ions of the ionic liquids.[12] Furthermore, the [TFSI] anions can hydrogen bond with the C-H or O-H CNF/CNC groups due to the S=O and C-F [TFSI] groups.[12, 35] Overall, XPS results confirmed intimate interactions between PIL/ionic liquid molecules and nanocellulose network frame in the solid films.

Next, thermogravitational analysis (TGA) for CNF showed an onset degradation (10% mass loss) temperature of 167ºC and maximum thermal decomposition at 200ºC which is in agreement with previous reports **Figure 4c** and **Figure S15**.[36] Pure ionic liquids exhibited onset and peak degradation temperatures at 424ºC and 476ºC, respectively. CNF/CNC ionogels and ionic liquids exhibited similar thermal due to high ionic liquid content (88 – 90 wt%). CNF/CNC/PIL-16 (IL) demonstrated an onset degradation temperature of 340ºC and peak degradation at 462ºC. Small improvements in degradation temperature with the addition of PILs with higher ionic group densities was observed. CNF/CNC/PIL-64 (IL) demonstrated an onset degradation of 410ºC with peak degradation at 471ºC. Higher thermal stability can be associated with the enhanced polymer-

nanocrystal interactions within the composite ionogels.[37] The high thermal stability of the CNF/CNC/PIL ionogels suggests that they could be utilized at high temperatures, up to 340 – 400ºC, that is critical for thermally stable energy storage devices.[1]

3.3 Mechanical properties and ionic conductivity

All CNF/CNC ionogels exhibited common stress-strain behavior for reinforced elastomeric materials with ultimate strain reaching 4% (**Figure 5, Figure S6** and **Table S1**). Despite the high ionic liquid content (88 – 90 wt%), the composite ionogels exhibited high Young's modulus (> 0.17 GPa) and tensile strength (> 1.2 MPa) resulting from the CNF continuous networks and the strong interfacial interactions between components within the composite ionogels.[12]

Addition of up to 0.5 wt% CNCs led to significant improvements in mechanical performance compared to the CNF (IL) ionogels. More specifically, CNF/0.25 wt% CNC (IL) demonstrated a Young's modulus of 0.24 ± 0.04 GPa (vs. 0.17 ± 0.01 GPa for CNF (IL)), a tensile strength of 3.2 ± 0.2 MPa (vs. 2.0 ± 0.5 MPa for CNF (IL)), an ultimate strain of 2.4 ± 0.4 % (vs. 2.0 ± 0.2% for CNF (IL)), and a toughness of 66 ± 23 kJ/m^3 (vs. 19 ± 1 kJ/m^3 for CNF (IL)). Similarly, CNF/0.5 wt% CNC (IL) exhibited a Young's modulus of 0.32 ± 0.03 GPa, a tensile strength of 6.2 ± 0.4 MPa, an ultimate strain of 2.6 ± 0.5%, and a toughness of 128 ± 10 kJ/m^3. The improvements in mechanical performance are attributed to the CNCs that strongly interact with the CNFs through hydrogen bonding and facilitate load transfer between components within the ionogels.[14] Additionally, a multistep plastic deformation with partial crack propagation at high strains was observed for the CNF/CNC ionogels (without PILs), because of possible cellulose nanofiber bridging and fiber reorientation, as observed in nanofiber reinforced composites.[38] Higher CNC loadings (0.75 wt%, 1.0 wt%, and 1.5 wt% explored in this study) led to an overall deteriorated mechanical performance due to possible CNC agglomerations that disrupt the continuous CNF networks (**Figure S6** and **Table S1**).[39]

Upon further addition of PILs, Young's modulus and tensile strength further increased significantly (22-fold and 8-fold, respectively) (**Figure 5** and **Table S1**). For example, CNF/0.5 wt% CNC/PIL-16 (IL) demonstrated a Young's modulus of 0.9 ± 0.1 GPa and a tensile strength of 11.0 ± 0.7 MPa. Addition of PILs with higher ionic group densities led to further enhancements with the CNF/CNC/PIL-32 (IL) gels exhibiting a Young's modulus of 1.9 ± 0.3 GPa and a tensile

strength of 14.2 ± 1.6 MPa. CNF/CNC/PIL-64 (IL) gels had a Young's modulus of 3.8 ± 0.7 GPa and a tensile strength of 17.2 ± 2.6 MPa.

The increasing Young's modulus and tensile strength are attributed to the strong interactions between CNF/CNC and the PILs, as discussed earlier. In contrast, ultimate strain and toughness did not follow the same trend. CNF/CNC/PIL-16 (IL) demonstrated an ultimate strain of 3.8 ± 0.5% and a toughness of 272 ± 30 kJ/m^3 which corresponds to a 2-fold and 14-fold improvement. The PIL-16 ionogel demonstrated a similar multistep plastic deformation with partial crack propagation to the CNF/CNC ionogels (without PILs) resulting from possible CNF bridging and reorientation.[40] On the other hand, composite ionogels with PIL-32 and PIL-64 became brittle and exhibited deteriorated toughness values (**Figure 5** and **Table S1**). This stiffening can be caused by entanglements of the long PIL terminal chains and the CNF interconnected networks, as well as their strong interfacial interactions.[41]

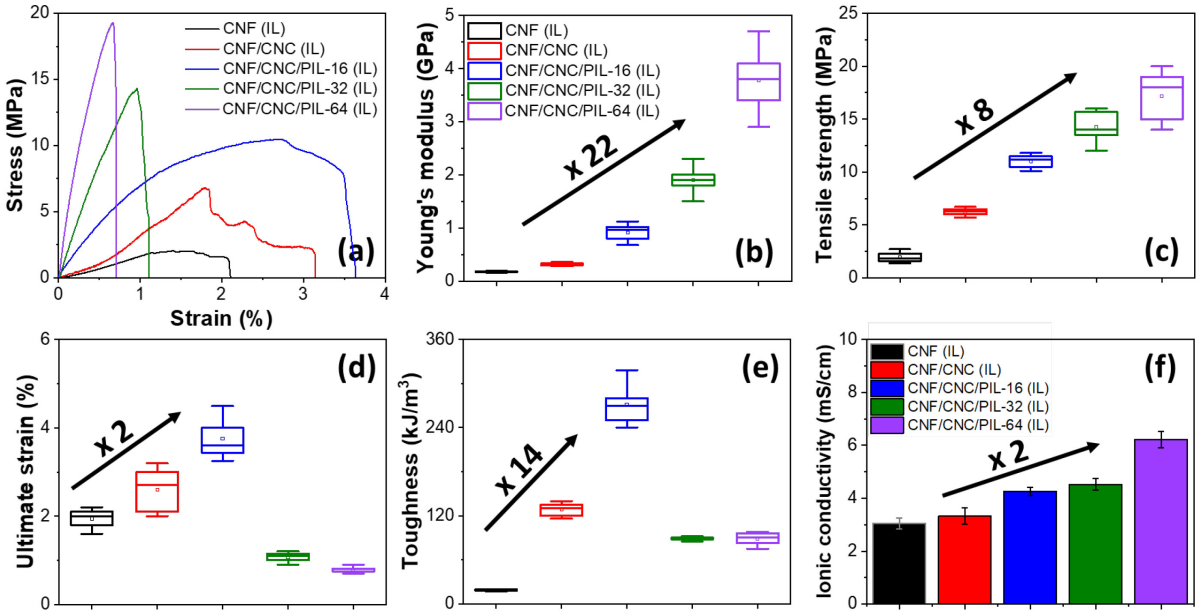

Figure 5. (a) Representative stress-strain curves, and box plots for (b) Young's modulus, (c) tensile strength, (d) ultimate strain, (e) toughness, and bar graph for (f) ionic conductivity for CNF (IL), CNF/CNC (IL), CNF/CNC/PIL-16 (IL), CNF/CNC/PIL-32 (IL), and CNF/CNC/PIL-64 (IL). Legend in panel (b) applies also for panels (c-e). Positions on the x-axis of the box plots correspond to different compositions as indicated by color coding in panel (b).

Finally, as known, pure ionic liquids ([EMIM][TFSI]) have been reported to have an ionic conductivity of 10.9 mS/cm.[42] Correspondingly, the CNF-based ionogels exhibited slightly

reduced ionic conductivity in the range of 3.0 – 6.2 mS/cm due to the high ionic liquid content and the open porous interconnected CNF network morphology (**Figure S16** and **Figure 5f**). Furthermore, an increase in ionic conductivity was observed upon addition of PIL components. More specifically, CNF/CNC (IL) ionogels demonstrated ionic conductivity of 3.3 ± 0.3 mS/cm, while CNF/CNC/PIL-16 (IL) had an ionic conductivity of 4.3 ± 0.2 mS/cm. Increasing the PIL ionic group density, ionic conductivity increased up to 6.2 ± 0.3 mS/cm (for CNF/CNC/PIL-64 (IL)). The improvement in ionic conductivity can be attributed to the screening of interfacial interactions of nanocellulose framework by absorbed PILs that facilitate ion liquid transport through open continuous pores with minimum dissipation of energy.[43, 44]

3.4 Energy storage performance demonstration

In order to test the practical performance of composite ionogels in device environment, we fabricated supercapacitors comprised of selected CNF-ionogels and reduced graphene oxide (rGO) electrodes that make them robust and bendable at the same time (**Figure 6a-c**). More specifically, we selected CNF/CNC/PIL-64 (IL) because it demonstrated the highest ionic conductivity and strength, CNF/CNC/PIL-16 (IL) due to its combination of good ionic conductivity and high toughness, and CNF (IL) as the control. All devices tested here exhibited pseudo-rectangular cyclic voltammograms (CVs) resulting from the formation of electric double layer (EDL) at the electrode/electrolyte interface (**Figure 6**, **Figure S17**, and **Table S6**).[45] Deviation from perfect rectangular CVs behavior indicates some ion-diffusion limitations, which are common for solid state devices based on ionic liquids due to the lower electrolyte ionic-conductivity and the large ionic liquid molecules.[12, 45]

First, CNF (IL)-containing supercapacitors exhibited a specific capacitance of 19.9 ± 1.2 F/g at 100 mV/s. Furthermore, supercapacitors with PIL-containing electrolytes demonstrated enhanced capacitance values and rate capabilities with capacitance values of 34.5 – 44.1 F/g at 100 mV/s resulting from the enhanced ion-conduction of ionic liquids through nanocellulose framework with the PIL modification. This is also confirmed by their superior ionic conductivity values (4.3 mS/cm for CNF/CNC/PIL-16 (IL) and 6.2 mS/cm for CNF/CNC/PIL-64 (IL) vs. 3.0 mS/cm for CNF (IL)) resulting from the ionically conductive PIL bearing groups that facilitate ion-transport. At increasing the scan rate, capacitance deteriorated due to ion-diffusion limitations.[12] Similar observations were made from galvanostatic charge-discharge experiments at various specific

currents (0.2 - 1 A/g, **Figure S18**). In conclusion, it is worth to note that similar characteristics were obtained for all supercapacitors at 1 mV/s with specific capacitance values of 117 – 120 F/g, which is comparable to rGO-based solid state supercapacitors.[46, 47]

Furthermore, CV was performed for these flexible supercapacitors in flat and bent states to test sustainability under deformations and the mechanical robustness of the CNF-based ionogels (**Figure 6d** and **Table S7**). More specifically, CV was performed at 50 mV/s for 10000 cycles with the state of the supercapacitor changing from flat to bent every 2000 cycles. In fact, the CNF (IL) and CNF/CNC/PIL-64 (IL) containing supercapacitors exhibited modest electrochemical stability against bending cycling with a capacitance retention of only ~50% and ~58% after 10000 cycles, respectively.

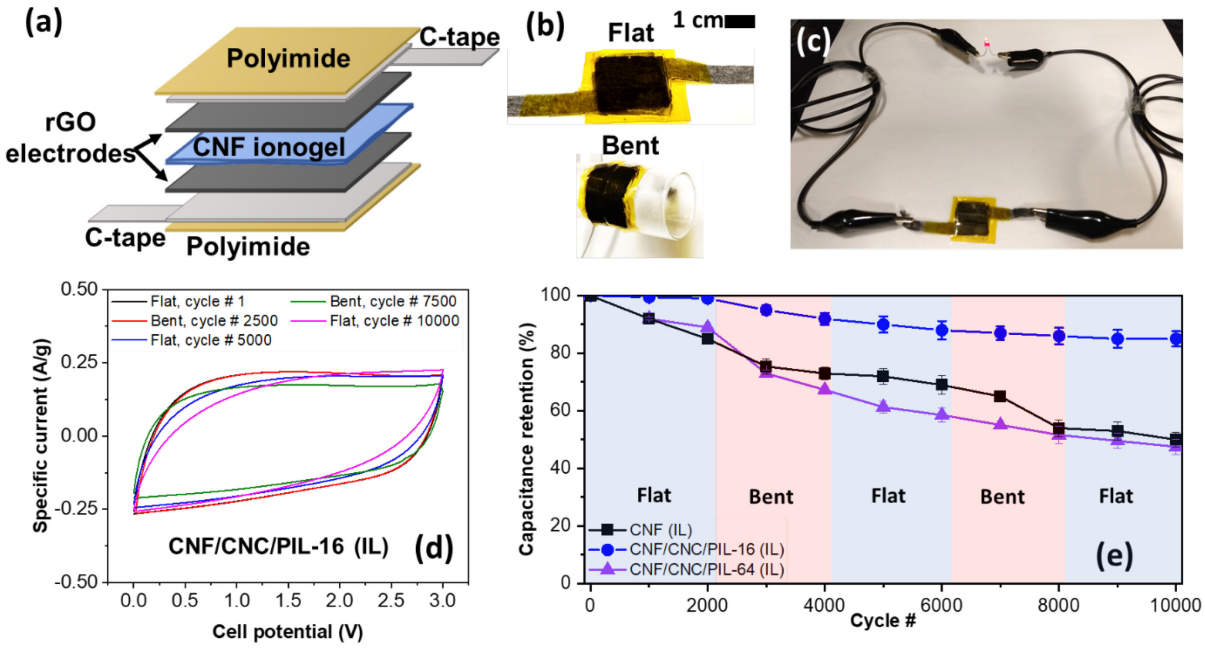

Figure 6. (a) Schematic representation and optical images of the (b) supercapacitor with the CNF-based ionogels and (c) the supercapacitor lighting up a red LED light. (c) Cyclic voltammetry at 50 mV/s for CNF/CNC/PIL-16 (IL) in flat and bent states (bending radius: 0.8 cm) and (d) capacitance retention vs. cycle number for CNF (IL), CNF/CNC/PIL-16 (IL), and CNF/CNC/PIL-64 (IL).

In contrast, the PIL-16 containing supercapacitors exhibited much enhanced electrochemical stability to severe bending deformations (bending radius of 0.8 cm) with a high capacitance retention of ~ 85% after 10000 cycles (**Figure 6e**). The improved capacitance retention under cycling deformation can be attributed to enhanced mechanical robustness, high toughness, and

strength of composite ionogels with PIL-16 acting as an interfacial agent between open porous nanocellulose frame and liquid phase immersed.[48,49]

3.5 Discussion

As has been discussed above, gel/solid electrolytes need to combine high ionic conductivity and high Young's modulus to accommodate for the current needs for safer flexible and stress-prone supercapacitors and batteries. High ionic conductivity is required to facilitate fast ion-transport and enhanced energy storage, while good mechanical properties accommodate enhanced safety against external and internal mechanical stresses and leaks.[50] Recent summary of corresponding performances in terms of ionic conductivities/specific energy vs elastic modulus is presented in **Figure 7**.[51] Young's modulus is of particular interest in the field of gel/solid electrolytes due to its correlation to the internally developed stresses during charging/discharging and prospective metal-ion dendrites growth suppression, for the case of metal-ion batteries.[50] It is worth noting that few studies would also report mechanical strength and toughness. On the other hand, the specific energy, which corresponds to the amount of energy stored, is one of the main performance metrics in addition to traditional ionic conductivity.[52]

Next, as known, the ionic conductivity and specific energy are inversely correlated to the Young's modulus [11, 51, 50] and attempts to improve ion-conduction typically leads to deteriorations in mechanical properties below common rubbery materials performance.[11, 51, 50] To date, only a handful of reports have demonstrated the simultaneous improvement of both ion-conduction and mechanical performance, and only modest improvements were achieved while the final energy storage performance is often overlooked. [51, 50, 53]

Indeed, as clear from this Ashby analysis of current reported results for ionogels (**Figure 7a** and **Table S8**), known solid polymer and polymer hybrid electrolytes demonstrate poor ion-conduction within 10^{-5} – 10^{-1} mS/cm resulting from the restricted segmental mobility of the ionically conductive polymer chains.[12, 48, 54, 55, 56] Their mechanical performance is characterized by wide range of Youngs' moduli from MPas to GPa. In contrast, current gel electrolytes offer enhanced ion-conduction, however, this comes with poor mechanical performance.[1] Specifically, gel electrolytes typically reach ionic conductivities of 10^{-2} – 10^{2} mS/cm with lower Young's moduli (in MPa range).[1] Recent attempts to improve the mechanical performance while maintaining high ionic conductivity using bi-continuous epoxy-based electrolytes and double-polymer crosslinked

networks led to gel electrolytes with Young's moduli of ~ 1 GPa and ionic conductivities of 1 – 40 mS/cm (**Figure 7a**).[11, 48] In contrast to reported result, CNF-based ionogels fabricated in this study surpassed this performance greatly with Young's moduli reaching 3.8 GPa, common for reinforced elastomeric polymer materials (**Figure 7a**).

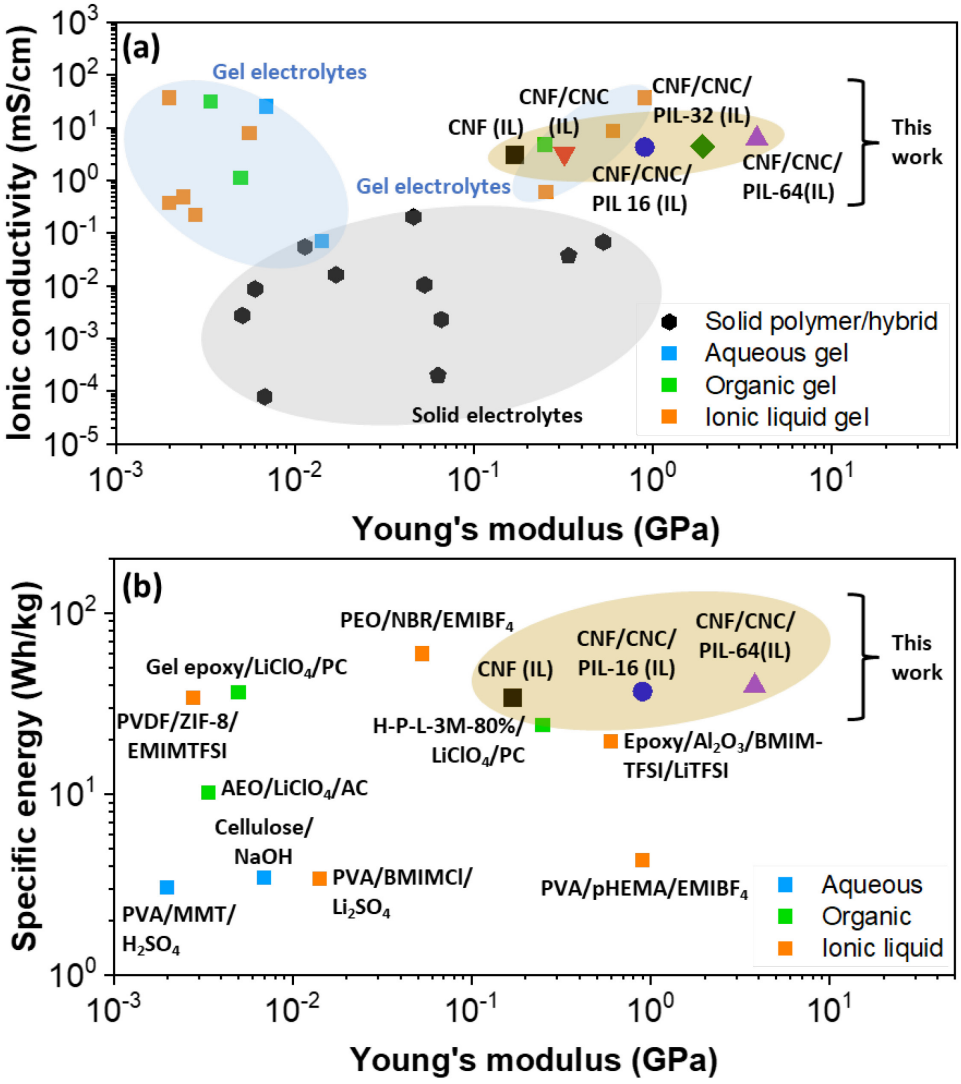

Figure 7. Ashby plots of ionogel materials performance: (a) Ionic conductivity vs. Young's modulus for solid and gel electrolytes. (b) Specific energy vs. electrolyte Young's modulus for supercapacitors containing gel-based electrolytes. **Tables S8 - S9** provide details and references.

The CNF-based ionogels maintained high ionic conductivity values (3.0 – 6.2 mS/cm in comparison with 10.9 S/cm for pure [EMIM][TFSI]).[41] Furthermore, increasing the ionic group density at the interface between nanocellulose frame and ionic liquid phase (with PIL-16 to PIL-

64 addition) resulted in significant improvements in both ion-conduction and mechanical performance (**Figure 7a**). Such unique behavior, in fact, breaks the traditional trade-off thus, placing them in a unique parametric space unachievable with traditional electrolyte materials and structures.

In addition, we conducted comparative analysis of the specific energy (Wh/kg) of supercapacitors containing different solid or gel electrolytes (**Figure 7b** and **Table S9**). The known electrolyte materials are categorized based on their solvent by aqueous, organic, and ionic liquid-based and emphasis was given to supercapacitors that used carbon-based electrodes (rGO and other carbon materials) for comparison reasons and to avoid any pseudocapacitive contributions.[11, 43, 52, 53] Comparison was conducted to other ionic liquid-based electrolytes reported to date, such as polyvinyl alcohol (PVA)/crosslinked poly(2-hydroxyethyl methacrylate) (C-pHEMA)/60 wt% $EMIMBF_4$,[48] polyvinylidene fluoride (PVDF)/ZIF-8/74 wt% EMITFSI,[54] polyoxyethylene/nitrile butadiene rubber (PEO/NBR) with 70 wt% $EMIBF_4$,[57] epoxy/Al_2O_3/50 wt% BMIM-TFSI/LiTFSI,[11] and PVA/35 wt% BMIMCl-Li_2SO_4 (**Figure 7b**).[48]

The CNF-based ionogels demonstrated comparable specific energy values (36.9 – 37.5 Wh/kg) resulting from the high ionic liquid content (88 – 90 wt%) and the porous CNF networks that accommodate ion-transport (**Figure 7b**). Only PEO/NBR with 70 wt% $EMIBF_4$ show higher specific energy values (59.4 Wh/kg) which can be associated to pseudocapacitive contributions from the nitrogen-doped carbon electrodes used in that case.[57] The highest modulus among the different polymer-based electrolytes used in supercapacitors was obtained for CNF/CNC/PIL-64 (3.8 GPa) due to the strong and continuous CNF/CNC networks with strongly interacting PIL-64 linker. At this point, it is worth noting that the PIL-16 containing ionogels also exhibited the highest toughness values (272 kJ/m^3) (**Table S1**).

Overall, CNF-based composite ionogels fabricated in this work exhibited a unique balanced energy storage and mechanical performance if compared with traditional polymer-based electrolyte materials. More specifically, the CNF-ionogels demonstrated improved energy storage and mechanical performance with the larger electrochemical stability potential window of the ionic liquids and the continuous and strong CNF/CNC/PIL networks.[48, 53, 54] We suggest that a key factor causing the enhanced performance is the presence of strong open and continuous porous networks

from cellulose nanofibers that facilitate mechanical robustness without compromising transport of large ionic molecules.

On the other hand, the addition of highly branched polymer ionic components with high concentration of ionic terminal groups screens the surface groups of nanofibers and nanocrystals and allows for enhanced transport of ionic molecules through porous networks. At the same time, we suggest that multiple hydrogen bonds between the PIL and nanofiber surfaces facilitate load transfer within the multicomponent material and ultimately leads to improved mechanical performance without compromising the sturdy open porous morphology. These interactions occur between the cellulose surface groups, the ionic liquid S=O and C-F [TFSI] groups, and the π^{+}-cloud in the PIL imidazolium ring.[12]

4. Conclusions

In conclusion, we demonstrated flexible, mechanically robust, and highly conductive composite ionogel electrolytes from a nanocellulose frame with added polymer ionic liquids. The highly porous and mechanically strong CNF/CNC networks host large amounts (up to 90 wt% vs. 50 – 85 wt% typically reported in the literature)[9,43,51,52] of ionic liquids while supporting robust, shape-persistent, flexible, and semi-transparent ionogel thin films, which are sustainable under prolonged cyclic deformational stresses. This combination of high ion-conduction and mechanical reinforcement can rarely be achieved as these properties come at a trade-off. To our knowledge, the effect of hyperbranched PIL ionic group density on the performance of ionogels was investigated for the first time. It was found that the PIL ionic group density can significantly affect the ionogel properties leading to multi-fold improvements in ion-conduction, energy storage, and mechanical performance. The greatly improved performance of the PIL-containing ionogels and their unique position in parametric space for existing polymer ionogels result from the balance of open porous morphology of strong nanocellulose networks and the ionically conductive PIL linkers. Efficient modification of porous network with branched polymer with high-density of terminal ionic/counter-ionic enables fast ion-transport and significantly reduces ionic liquid energy dissipation for ion transport. Correspondingly, we verified that these composite ionogels have the potential to be used as robust bendable electrolyte media in stress-sustainable energy storage devices such as flexible supercapacitors capable of sustainable performance under cycling abusive bending deformations.

Overall, we suggest that this work offers insights on fabrication of composite gel electrolytes with unique electromechanical and mechanical performance that paves the pathway for the development of both conductive and mechanically robust gel electrolytes for high-energy storage devices sustainable under cyclical stresses. The nanocellulose-based composite ionogels can be further investigated using different ionic liquid and PIL chemistries and architectures, and they can be considered for prospective applications such as in wearable power sources, self-powered electrochemical sensors, and actuating elastomeric materials for soft robotics.

ASSOCIATED CONTENT

Supporting Information. Supporting Information is available free of charge at https://pubs.acs.org/doi/xx.xxxx. Contains optical images of the ionogels, mechanical and electrochemical measurements, and additional characterizations.

AUTHOR INFORMATION

Corresponding author

Vladimir V. Tsukruk - School of Materials Science and Engineering, Georgia Institute of Technology, Atlanta, Georgia 30332, USA.

E-mail: vladimir@mse.gatech.edu

Author Contributions

The manuscript was written through contributions of all authors. All authors have given approval to the final version of the manuscript.

Funding Sources

This study is supported by the National Science Foundation DMR 2001968, the Air Force Research Laboratory grant FA8650-D-16-5404 and Air Force Office for Scientific Research grant FA9550-20-1-0305.

Notes

There are no conflicts to declare.

ACKNOWLEDGMENTS

The authors thank A. Filippas and Prof. N. Liu for help with EIS.

REFERENCES

(1) Zhou, D.; Shanmukaraj, D.; Tkacheva, A.; Armand, M.; Wang, G. Polymer Electrolytes for Lithium-Based Batteries: Advances and Prospects. *Chem* **2019,** *5* (9), 2326-2352, DOI: https://doi.org/10.1016/j.chempr.2019.05.009.

(2) Osada, I.; de Vries, H.; Scrosati, B.; Passerini, S. Ionic-Liquid-Based Polymer Electrolytes for Battery Applications. *Angew. Chem. Int. Ed.* **2016,** *55* (2), 500-513, DOI: https://doi.org/10.1002/anie.201504971

(3) Watanabe, M.; Thomas, M. L.; Zhang, S.; Ueno, K.; Yasuda, T.; Dokko, K. Application of Ionic Liquids to Energy Storage and Conversion Materials and Devices. *Chem. Rev.* **2017,** *117* (10), 7190-7239, DOI: 10.1021/acs.chemrev.6b00504.

(4) Rakov, D. A.; Chen, F.; Ferdousi, S. A.; Li, H.; Pathirana, T.; Simonov, A. N.; Howlett, P. C.; Atkin, R.; Forsyth, M. Engineering High-Energy-Density Sodium Battery Anodes for Improved Cycling with Superconcentrated Ionic-Liquid Electrolytes. *Nat. Mater.* **2020,** *19* (10), 1096-1101, DOI: 10.1038/s41563-020-0673-0.

(5) Sun, H.; Zhu, G.; Zhu, Y.; Lin, M.-C.; Chen, H.; Li, Y.-Y.; Hung, W. H.; Zhou, B.; Wang, X.; Bai, Y.; Gu, M.; Huang, C.-L.; Tai, H.-C.; Xu, X.; Angell, M.; Shyue, J.-J.; Dai, H. High-Safety and High-Energy-Density Lithium Metal Batteries in a Novel Ionic-Liquid Electrolyte. *Adv. Mater.* **2020,** *32* (26), 2001741, DOI: https://doi.org/10.1002/adma.202001741..

(6) Yang, Q.; Zhang, Z.; Sun, X.-G.; Hu, Y.-S.; Xing, H.; Dai, S. Ionic Liquids and Derived Materials for Lithium and Sodium Batteries. *Chem. Soc. Rev.* **2018,** *47* (6), 2020-2064, DOI: 10.1039/C7CS00464H.

(7) Eshetu, G. G.; Mecerreyes, D.; Forsyth, M.; Zhang, H.; Armand, M. Polymeric Ionic Liquids for Lithium Based Rechargeable Batteries. *Mol. Sys. Des. Eng.* **2019,** *4* (2), 294-309, DOI: 10.1039/C8ME00103K.

(8) Xu, W.; Ledin, P. A.; Shevchenko, V. V.; Tsukruk, V. V. Architecture, Assembly, and Emerging Applications of Branched Functional Polyelectrolytes and Poly(Ionic Liquid)S. *ACS Appl. Mater. Interfaces* **2015,** *7* (23), 12570-12596, DOI: 10.1021/acsami.5b01833.

(9) Tomé, L. C.; Porcarelli, L.; Bara, J. E.; Forsyth, M.; Mecerreyes, D. Emerging Iongel Materials Towards Applications in Energy and Bioelectronics. *Mater. Horiz.* **2021,** *8* (12), 3239-3265, DOI: 10.1039/D1MH01263K.

(10) Chen, N.; Zhang, H.; Li, L.; Chen, R.; Guo, S. Ionogel Electrolytes for High-Performance Lithium Batteries: A Review. *Adv. Energy Mater.* **2018,** *8* (12), 1702675, DOI: https://doi.org/10.1002/aenm.201702675.

(11) Kwon, S. J.; Kim, T.; Jung, B. M.; Lee, S. B.; Choi, U. H. Multifunctional Epoxy-Based Solid Polymer Electrolytes for Solid-State Supercapacitors. *ACS Appl. Mater. Interfaces* **2018,** *10* (41), 35108-35117, DOI: 10.1021/acsami.8b11016.

(12) Lee, H.; Erwin, A.; Buxton, M. L.; Kim, M.; Stryutsky, A. V.; Shevchenko, V. V.; Sokolov, A. P.; Tsukruk, V. V. Shape Persistent, Highly Conductive Ionogels from Ionic Liquids Reinforced with Cellulose Nanocrystal Network. *Adv. Funct. Mater.* **2021,** *31* (38), 2103083, DOI: https://doi.org/10.1002/adfm.202103083.

(13) Simotwo, S. K.; Chinnam, P. R.; Wunder, S. L.; Kalra, V. Highly Durable, Self-Standing Solid-State Supercapacitor Based on an Ionic Liquid-Rich Ionogel and Porous Carbon Nanofiber Electrodes. *ACS Appl. Mater. Interfaces* **2017,** *9* (39), 33749-33757, DOI: 10.1021/acsami.7b07479.

(14) Zhang, X.; Xiong, R.; Kang, S.; Yang, Y.; Tsukruk, V. V. Alternating Stacking of Nanocrystals and Nanofibers into Ultrastrong Chiral Biocomposite Laminates. *ACS Nano* **2020,** *14* (11), 14675-14685, DOI: 10.1021/acsnano.0c06192.

(15) Lee, H.; Stryutsky, A. V.; Korolovych, V. F.; Mikan, E.; Shevchenko, V. V.; Tsukruk, V. V. Transformations of Thermosensitive Hyperbranched Poly(Ionic Liquid)S Monolayers. *Langmuir* **2019,** *35* (36), 11809-11820, DOI: 10.1021/acs.langmuir.9b01905.

(16) Habibi, Y.; Lucia, L. A.; Rojas, O. J. Cellulose Nanocrystals: Chemistry, Self-Assembly, and Applications. *Chem. Rev.* **2010,** *110* (6), 3479-3500, DOI: 10.1021/cr900339w.
(17) Lee, H.; Rho, J.; Messersmith, P. B. Facile Conjugation of Biomolecules onto Surfaces Via Mussel Adhesive Protein Inspired Coatings. *Adv. Mater.* **2009,** *21* (4), 431-434, DOI: https://doi.org/10.1002/adma.200801222.
(18) Smith, M.; Scudiero, L.; Espinal, J.; McEwen, J.-S.; Garcia-Perez, M. Improving the Deconvolution and Interpretation of XPS Spectra from Chars by Ab Initio Calculations. *Carbon* **2016,** *110*, 155-171, DOI: https://doi.org/10.1016/j.carbon.2016.09.012.
(19) Yuan, H.; Nishiyama, Y.; Wada, M.; Kuga, S. Surface Acylation of Cellulose Whiskers by Drying Aqueous Emulsion. *Biomacromolecules* **2006,** *7* (3), 696-700, DOI: 10.1021/bm050828j.
(20) McConney, M. E.; Singamaneni, S.; Tsukruk, V. V. Probing Soft Matter with the Atomic Force Microscopies: Imaging and Force Spectroscopy. *Polym. Rev.* **2010,** *50* (3), 235-286, DOI: 10.1080/15583724.2010.493255.
(21) Wang, C.; Huang, D.; Li, S.; Yu, J.; Zhu, M.; Liu, N.; Lu, Z. Three-Dimensional-Percolated Ceramic Nanoparticles Along Natural-Cellulose-Derived Hierarchical Networks for High Li+ Conductivity and Mechanical Strength. *Nano Lett.* **2020,** *20* (10), 7397-7404, DOI: 10.1021/acs.nanolett.0c02721.
(22) Ma, R.; Gordon, D.; Yushin, G.; Tsukruk, V. V. Robust and Flexible Micropatterned Electrodes and Micro-Supercapacitors in Graphene–Silk Biopapers. *Adv. Mater. Interfaces* **2018,** *5* (24), 1801203, DOI: https://doi.org/10.1002/admi.201801203.
(23) Hummers, W. S.; Offeman, R. E. Preparation of Graphitic Oxide. *J. Am. Chem. Soc.* **1958,** *80* (6), 1339-1339, DOI: 10.1021/ja01539a017.
(24) Kwon, S. R.; Harris, J.; Zhou, T.; Loufakis, D.; Boyd, J. G.; Lutkenhaus, J. L. Mechanically Strong Graphene/Aramid Nanofiber Composite Electrodes for Structural Energy and Power. *ACS Nano* **2017,** *11* (7), 6682-6690, DOI: 10.1021/acsnano.7b00790.
(25) Shevchenko, V. V.; Stryutsky, A. V.; Klymenko, N. S.; Gumenna, M. A.; Fomenko, A. A.; Bliznyuk, V. N.; Trachevsky, V. V.; Davydenko, V. V.; Tsukruk, V. V. Protic and Aprotic Anionic Oligomeric Ionic Liquids. *Polymer* **2014,** *55* (16), 3349-3359, DOI: https://doi.org/10.1016/j.polymer.2014.04.020.
(26) Korolovych, V. F.; Erwin, A.; Stryutsky, A.; Lee, H.; Heller, W. T.; Shevchenko, V. V.; Bulavin, L. A.; Tsukruk, V. V. Thermally Responsive Hyperbranched Poly(Ionic Liquid)S: Assembly and Phase Transformations. *Macromolecules* **2018,** *51* (13), 4923-4937, DOI: 10.1021/acs.macromol.8b00845.
(27) Hess, M.; Jones, R. G.; Kahovec, J.; Kitayama, T.; Kratochvíl, P.; Kubisa, P.; Mormann, W.; Stepto, R. F. T.; Tabak, D.; Vohlídal, J.; Wilks, E. S. Terminology of Polymers Containing Ionizable or Ionic Groups and of Polymers Containing Ions (Iupac Recommendations 2006). *Pure Appl. Chem.* **2006,** *78* (11), 2067-2074, DOI: 10.1351/pac200678112067.
(28) Kim, M.; Pierce, K.; Krecker, M.; Bukharina, D.; Adstedt, K.; Nepal, D.; Bunning, T.; Tsukruk, V. V. Monolithic Chiral Nematic Organization of Cellulose Nanocrystals under Capillary Confinement. *ACS Nano* **2021,** *15* (12), 19418-19429, DOI: 10.1021/acsnano.1c05988.
(29) Koç, B.; Eren, İ.; Kaymak Ertekin, F. Modelling Bulk Density, Porosity and Shrinkage of Quince During Drying: The Effect of Drying Method. *J. Food Eng.* **2008,** *85* (3), 340-349, DOI: https://doi.org/10.1016/j.jfoodeng.2007.07.030.
(30) Kang, K.-Y.; Hwang, K.-R.; Park, J.-Y.; Lee, J.-P.; Kim, J.-S.; Lee, J.-S. Critical Point Drying: An Effective Drying Method for Direct Measurement of the Surface Area of a Pretreated Cellulosic Biomass. *Polymers* **2018,** *10* (6), 676, DOI: 10.3390/polym10060676
(31) Kiefer, J.; Fries, J.; Leipertz, A. Experimental Vibrational Study of Imidazolium-Based Ionic Liquids: Raman and Infrared Spectra of 1-Ethyl-3-Methylimidazolium Bis(Trifluoromethylsulfonyl)Imide and 1-Ethyl-3-Methylimidazolium Ethylsulfate. *Appl. Spectrosc.* **2007,** *61* (12), 1306-1311, DOI: 10.1366/000370207783292000
(32) Bulota, M.; Tanpichai, S.; Hughes, M.; Eichhorn, S. J. Micromechanics of Tempo-Oxidized Fibrillated Cellulose Composites. *ACS Appl. Mater. Interfaces* **2012,** *4* (1), 331-337, DOI: 10.1021/am201399q.

(33) Huang, P.; Zhao, Y.; Kuga, S.; Wu, M.; Huang, Y. A Versatile Method for Producing Functionalized Cellulose Nanofibers and Their Application. *Nanoscale* **2016,** *8* (6), 3753-3759, DOI: 10.1039/C5NR08179C.
(36) Clarke, C. J.; Maxwell-Hogg, S.; Smith, E. F.; Hawker, R. R.; Harper, J. B.; Licence, P. Resolving X-Ray Photoelectron Spectra of Ionic Liquids with Difference Spectroscopy. *Phys. Chem. Chem. Phys.* **2019,** *21* (1), 114-123, DOI: 10.1039/C8CP06701E.
(35) Mao, J. X.; Nulwala, H. B.; Luebke, D. R.; Damodaran, K. Spectroscopic and Computational Analysis of the Molecular Interactions in the Ionic Liquid Ion Pair [Bmp]+[Tfsi]−. *J. Mol. Liq.* **2012,** *175*, 141-147, DOI: https://doi.org/10.1016/j.molliq.2012.09.001.
(36) Soni, B.; Hassan, E. B.; Mahmoud, B. Chemical Isolation and Characterization of Different Cellulose Nanofibers from Cotton Stalks. *Carbohydr. Polym.* **2015,** *134*, 581-589, DOI: https://doi.org/10.1016/j.carbpol.2015.08.031.
(37) Yuan, X. Enhanced Interfacial Interaction for Effective Reinforcement of Poly(Vinyl Alcohol) Nanocomposites at Low Loading of Graphene. *Polym. Bul.* **2011,** *67* (9), 1785-1797, DOI: 10.1007/s00289-011-0506-z.
(38) Wegst, U. G. K.; Bai, H.; Saiz, E.; Tomsia, A. P.; Ritchie, R. O. Bioinspired Structural Materials. *Nat. Mater.* **2015,** *14* (1), 23-36, DOI: 10.1038/nmat4089.
(39) Qin, S.; Hu, Y.; Tian, X.; Tian, Y.; Liu, W.; Zhao, L. Modification of Cellulose Nanocrystals by Self-Assembly Nucleation Agents to Improve Poly(L-Lactide) Nanocomposite' Properties. *Cellulose* **2020,** *27* (8), 4337-4353, DOI: 10.1007/s10570-020-03069-x.
(40) Kurniawan, N. A.; Wong, L. H.; Rajagopalan, R. Early Stiffening and Softening of Collagen: Interplay of Deformation Mechanisms in Biopolymer Networks. *Biomacromolecules* **2012,** *13* (3), 691-698, DOI: 10.1021/bm2015812.
(41) Lossada, F.; Jiao, D.; Guo, J.; Hoenders, D.; Eckert, A.; Walther, A. Outstanding Synergies in Mechanical Properties of Bioinspired Cellulose Nanofibril Nanocomposites Using Self-Cross-Linking Polyurethanes. *ACS Appl. Mater. Interfaces* **2019,** *1* (12), 3334-3342, DOI: 10.1021/acsapm.9b00774.
(42) Horowitz, A. I.; Panzer, M. J. High-Performance, Mechanically Compliant Silica-Based Ionogels for Electrical Energy Storage Applications. *J. Mater. Chem.* **2012,** *22* (32), 16534-16539, DOI: 10.1039/C2JM33496H.
(43) Gao, T.; Itliong, J.; Kumar, S. P.; Hjorth, Z.; Nakamura, I. Polarization of Ionic Liquid and Polymer and Its Implications for Polymerized Ionic Liquids: An Overview Towards a New Theory and Simulation. *J. Polym. Sci.* **2021,** *59* (21), 2434-2457, DOI: https://doi.org/10.1002/pol.20210330.
(44) Evans, C. M.; Sanoja, G. E.; Popere, B. C.; Segalman, R. A. Anhydrous Proton Transport in Polymerized Ionic Liquid Block Copolymers: Roles of Block Length, Ionic Content, and Confinement. *Macromolecules* **2016,** *49* (1), 395-404, DOI: 10.1021/acs.macromol.5b02202.
(45) Guo, S.; Zhao, K.; Feng, Z.; Hou, Y.; Li, H.; Zhao, J.; Tian, Y.; Song, H. High Performance Liquid Crystalline Bionanocomposite Ionogels Prepared by in Situ Crosslinking of Cellulose/Halloysite Nanotubes/Ionic Liquid Dispersions and Its Application in Supercapacitors. *Appl. Surf. Sci.* **2018,** *455*, 599-607, DOI: https://doi.org/10.1016/j.apsusc.2018.06.026.
(46) Li, S.; Zhao, C.; Shu, K.; Wang, C.; Guo, Z.; Wallace, G. G.; Liu, H. Mechanically Strong High Performance Layered Polypyrrole Nano Fibre/Graphene Film for Flexible Solid State Supercapacitor. *Carbon* **2014,** *79*, 554-562, DOI: https://doi.org/10.1016/j.carbon.2014.08.014.
(47) Luo, J.; Jang, H. D.; Huang, J. Effect of Sheet Morphology on the Scalability of Graphene-Based Ultracapacitors. *ACS Nano* **2013,** *7* (2), 1464-1471, DOI: 10.1021/nn3052378.
(48) Lu, C.; Chen, X. All-Temperature Flexible Supercapacitors Enabled by Antifreezing and Thermally Stable Hydrogel Electrolyte. *Nano Lett.* **2020,** *20* (3), 1907-1914, DOI: 10.1021/acs.nanolett.9b05148.
(49) Rana, H. H.; Park, J. H.; Ducrot, E.; Park, H.; Kota, M.; Han, T. H.; Lee, J. Y.; Kim, J.; Kim, J.-H.; Howlett, P.; Forsyth, M.; MacFarlane, D.; Park, H. S. Extreme Properties of Double Networked Ionogel Electrolytes for Flexible and Durable Energy Storage Devices. *Energy Stor. Mater.* **2019,** *19*, 197-205, DOI: https://doi.org/10.1016/j.ensm.2018.11.008.

(50) Lin, D.; Yuen, P. Y.; Liu, Y.; Liu, W.; Liu, N.; Dauskardt, R. H.; Cui, Y. A Silica-Aerogel-Reinforced Composite Polymer Electrolyte with High Ionic Conductivity and High Modulus. *Adv. Mater.* **2018,** *30* (32), 1802661, DOI: https://doi.org/10.1002/adma.201802661.
(51) D'Angelo, A. J.; Panzer, M. J. Decoupling the Ionic Conductivity and Elastic Modulus of Gel Electrolytes: Fully Zwitterionic Copolymer Scaffolds in Lithium Salt/Ionic Liquid Solutions. *Adv. Energy Mater.* **2018,** *8* (26), 1801646, DOI: https://doi.org/10.1002/aenm.201801646.
(52) Simon, P.; Gogotsi, Y. Perspectives for Electrochemical Capacitors and Related Devices. *Nat. Mater.* **2020,** *19* (11), 1151-1163, DOI: 10.1038/s41563-020-0747-z.
(53) Wang, H.; Wu, J.; Qiu, J.; Zhang, K.; Shao, J.; Yan, L. In Situ Formation of a Renewable Cellulose Hydrogel Electrolyte for High-Performance Flexible All-Solid-State Asymmetric Supercapacitors. *Sustain. Energy Fuels* **2019,** *3* (11), 3109-3115, DOI: 10.1039/C9SE00339H.
(54) Lu, C.; Chen, X. Sea-Island Nanostructured Polyvinylidene Fluoride/Zeolitic Imidazolate Framework-8 Polyelectrolyte for High-Performance All-Solid-State Supercapacitors. *J. Power Sources* **2020,** *448*, 227587, DOI: https://doi.org/10.1016/j.jpowsour.2019.227587.
(55) Snyder, J. F.; Carter, R. H.; Wetzel, E. D. Electrochemical and Mechanical Behavior in Mechanically Robust Solid Polymer Electrolytes for Use in Multifunctional Structural Batteries. *Chem. Mater.* **2007,** *19* (15), 3793-3801, DOI: 10.1021/cm070213o.
(56) Liu, C.; Wang, J.; Kou, W.; Yang, Z.; Zhai, P.; Liu, Y.; Wu, W.; Wang, J. A Flexible, Ion-Conducting Solid Electrolyte with Vertically Bicontinuous Transfer Channels toward High Performance All-Solid-State Lithium Batteries. *Chemical Engineering Journal* **2021,** *404*, 126517, DOI: https://doi.org/10.1016/j.cej.2020.126517.
(57) Lu, C.; Wang, D.; Zhao, J.; Han, S.; Chen, W. A Continuous Carbon Nitride Polyhedron Assembly for High-Performance Flexible Supercapacitors. *Adv. Funct. Mater.* **2017,** *27* (8), 1606219, DOI: https://doi.org/10.1002/adfm.201606219.